High-order harmonic generation from diatomic molecules in an orthogonally polarized two-color laser field

Bing Zhang [1,2] and Manfred Lein [2]
[1] *School of Physics, Harbin Institute of Technology, 150001 Harbin, China*
[2] *Leibniz Universität Hannover, Appelstraβe 2, D-30167 Hannover, Germany*

(Received 1 June 2019; published 2 October 2019)

We study high-order harmonic generation (HHG) from aligned H_2^+ and oriented HeH^{2+} and HeH^+ molecular ions in orthogonally polarized two-color laser pulses composed of an intense fundamental field and a time-delayed weak second-harmonic field. By numerical solution of the time-dependent Schrödinger equation, we find that for a fixed alignment angle, as the delay between the two colors varies on a subcycle scale, the HHG intensity from H_2^+ shows a pronounced groove in a specific delay region, which turns out to be a two-center interference effect. HHG from asymmetric molecules shows an obvious orientation dependence where the interference effect can be observed only when the tunneling occurs on the helium side. The physical origin of these phenomena is deduced by modeling the two-color HHG intensity of H_2^+ using classical and quantum models and by modeling that of asymmetric molecules with the help of field-free collisions of Gaussian wave packets with the core.

DOI: 10.1103/PhysRevA.100.043401

I. INTRODUCTION

In recent years, high harmonic generation (HHG) has been a topic of wide interest in intense-laser matter interaction because of its potential application as an extreme ultraviolet light source [1]. The HHG process can be well understood using the three-step model [2]: (1) tunneling ionization, (2) electron acceleration in the external field, and (3) electron recombination with the core, emitting a high-energy photon. A quantum description of HHG is given by the quantum-orbit (QO) model [3], in which each harmonic emission frequency is attributed to a few dominant quantum trajectories [4]. The QO model has been well confirmed by both experiments [5] and theoretical work based on the time-dependent Schrödinger equations [6].

Molecular HHG encodes information about molecular structure, which facilitates imaging of the molecular orbitals using HHG [7,8]. Moreover, numerous interesting effects can be observed in HHG from diatomic molecules such as two-center interference [9–11] and orientation effects [12]. Due to two-center interference, a minimum appears in the HHG spectra of certain symmetric molecules and the position of the minimum is related to the orientation of the molecule [9]. This interference effect is a special case of the sensitivity of the recombination step to molecular structure which is used in molecular orbital tomography [7,13].

HHG can be controlled by introducing a second-harmonic field with orthogonal polarization that causes a transverse offset in the electron trajectories. With comparable strength of the two colors, the control of the tunneling electron [14] and orbital tomography using single-shot measurement [15] have been proposed. Furthermore, the timing and direction of the recollision in HHG as a function of subcycle delay between two colors has been discussed [16]. However, when the second-harmonic field is relatively weak, the timing of HHG is determined by the fundamental field. In this case, the two-color scheme can be used as a detecting scheme for HHG properties. By scanning the delay between the two fields and analyzing the observables, the reconstruction of ionization and recollision times has been achieved [6,17]. Most of the above work has focused on atoms, while HHG from molecules in two-color fields still holds many open questions.

In this article, we study HHG from models of diatomic molecular ions H_2^+, HeH^{2+}, and HeH^+ in orthogonally polarized two-color laser pulses. The TDSE is numerically solved with variable two-color delay. Our simulations show that for H_2^+, an apparent groove appears in the HHG intensity distribution as a function of the two-color delay and harmonic order. A similar but shallower groove can be observed in HHG from the asymmetric molecules when the tunneling occurs on the helium side. Our analysis reveals that these grooves arise from the two-center interference, the mechanism of which is slightly different in symmetric and asymmetric molecules. We model HHG from H_2^+ by considering the transverse effects induced by the second-harmonic field in combination with two-center interference. Using field-free collisions of Gaussian wave packets [9,18] and considering the orientation dependence of the ionization, we reach an understanding of the orientation asymmetry in HHG from asymmetric molecules.

This paper is organized as follows. We describe the details of the two-color calculation using the time-dependent Schrödinger equation (TDSE) in Sec. II. In Sec. III we report our main results and analyze the underlying mechanisms. Section IV presents our conclusions.

II. TDSE SIMULATION DETAILS

We work with the single-active-electron Hamiltonian $H(t) = \mathbf{p}^2/2 + V(\mathbf{r}) + \mathbf{r}\cdot\mathbf{E}(t)$ (using atomic units $\hbar = e =$

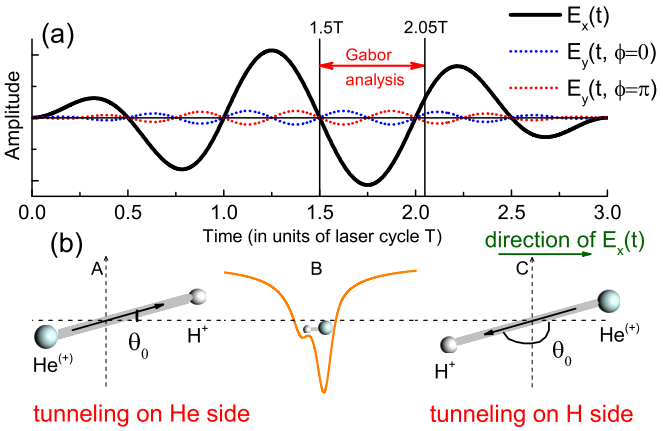

FIG. 1. (a) Time-dependent field of the orthogonally polarized two-color laser pulse, which consists of a fundamental field $E_x(t)$ (solid black curve) and a second-harmonic field $E_y(t)$ (red and blue dashed curves). The time domain of the Gabor analysis is marked by two vertical lines. (b) The orientation of the HeH^+ or HeH^{2+} molecule relative to the direction of $E_x(t)$ in the cases of the tunneling on the helium and hydrogen side. The field-free potential of HeH^+ is plotted in the middle.

$m_e = 1$). The external field is a trapezoidally shaped laser pulse with a total duration of three optical cycles and linear ramps of one cycle in the form

$$\mathbf{E}(t) = E_0 f(t)[\mathbf{e}_x \sin(\omega t) + \mathbf{e}_y \varepsilon \sin(2\omega t + \phi)]. \quad (1)$$

This pulse is composed of a fundamental field with amplitude E_0 and frequency ω and a weak second-harmonic field polarized perpendicularly with a relative amplitude $\varepsilon = 0.1$. The x and y components of the field are shown in Fig. 1(a). The phase ϕ has the role of the delay between the two colors and is scanned from 0 to 2π in steps of 1.0° (about 0.01745 rad). Two-dimensional (2D) calculations are adopted throughout our work, since the main properties of HHG from aligned or oriented molecules can be modeled in 2D.

The TDSE is numerically solved by the split-operator method [19]. The fundamental field is linearly polarized along the x axis, and the grid dimensions are $L_x \times L_y = 204.8 \times 102.4$ a.u. with 1024×512 grid points. After each time step, the TDSE wave function $\Psi(t)$ is multiplied by mask functions for each dimension to absorb the continuum wave packet at the boundary. The mask function along the x axis has the form $F(x) = \cos^{1/8}[\pi(|x| - x_0)/(L_x - 2x_0)]$ for $|x| \geqslant x_0$ and $F(x) = 1$ for $|x| \leqslant x_0$. According to the three-step model, long and short electronic trajectories contribute to HHG in each laser cycle. The interference of these different trajectories influences significantly the harmonic emission. To exclude this influence, in the following, we restrict our analysis to short trajectories which dominate the experimental HHG. This is achieved by setting the boundary of the absorbing procedure along the x direction (the direction of the fundamental field polarization) as $x_0 = 1.1E_0/\omega_0^2$ [20] to filter out the continuum wave packets related to the long trajectories. A similar treatment is used in y dimension with $y_0 = 3L_y/8$.

Once the dipole acceleration $\mathbf{a}(t)$ has been obtained, the Gabor time-frequency analysis [21,22] is implemented separately for the x and y components,

$$I_{G_{x(y)}}(\Omega, t) = \left| \int dt' a_{x(y)}(t') e^{-(t-t')^2/(2\sigma^2) + i\Omega t'} \right|^2. \quad (2)$$

Here we choose $\sigma = 1/(3\omega)$. The total Gabor intensity $I_G(\Omega, t) = I_{G_x}(\Omega, t) + I_{G_y}(\Omega, t)$ represents the intensity of one harmonic with frequency Ω emitted at time t. In the ultrashort laser pulse, the short trajectories that are born in the first half-cycle of the central part of the pulse contribute significantly to all harmonic orders. By taking the time window as $t = [1.5T, 2.05T]$, we isolate the HHG intensity coming from these trajectories ionizing (and recolliding) on the left side of the molecule. We define the emission time t_r of one harmonic Ω as the time corresponding to the local maximum of the Gabor intensity. $I_G(\Omega, t_r)$ can be regarded as the harmonic intensity and is strongly delay dependent. For each harmonic order, we find a maximum of harmonic intensity at a certain delay. In the two-color delay scan, the harmonic intensity is normalized separately for each harmonic order, and a normalized HHG intensity distribution depending on delay and harmonic order is obtained. In our calculations below, the Gabor analysis is applied only to the TDSE simulations with laser field, not to the Gaussian wave packet model described in Sec. III B, but the above-described normalization scheme is used throughout this paper.

A soft-core potential is used for the diatomic molecular ion,

$$V(\mathbf{r}) = -Z_1/\sqrt{\xi + r_1^2} - Z_2/\sqrt{\xi + r_2^2}. \quad (3)$$

Here the soft-core parameter $\xi = 0.5$ is used throughout this article. The squared distances from the nuclei are $r_1^2 = (x - R_1 \cos\theta_0)^2 + (y - R_1 \sin\theta_0)^2$ and $r_2^2 = (x + R_2 \cos\theta_0)^2 + (y + R_2 \sin\theta_0)^2$. Z_1 and Z_2 are effective charges, $R_1 = Z_2 R/(Z_1 + Z_2)$ and $R_2 = Z_1 R/(Z_1 + Z_2)$. R is the internuclear separation. θ_0 denotes the angle between molecular axis and the polarization of fundamental field. If $Z_1 = Z_2$, the above Hamiltonian represents a symmetric molecule where θ_0 is the alignment angle in the range from 0 to $\pi/2$. For asymmetric molecules, θ_0 is the orientation angle, and it is varied in the range from 0 to π.

III. RESULTS AND DISCUSSION

A. Symmetric molecular ion and tunneling-recombination model

For H_2^+ the effective charges are $Z_1 = Z_2 = 1$ a.u, the internuclear distance is $R = 2$ a.u., and the ionization potential is $I_p = 1.1$ a.u. The field strength is $E_0 = 0.1196$ a.u. corresponding to an intensity of $I = 5 \times 10^{14}$ W/cm^2, while the frequency $\omega = 0.05695$ a.u. corresponds to a wavelength of $\lambda = 800$ nm. Figure 2(a) gives an example of the HHG intensity distribution for parallel alignment (alignment angle $\theta_0 = 0^\circ$). The distribution shows two branches, and the HHG intensity is periodic in the delay ϕ with period π, which is similar to the atomic case [6]. However, the two-color scan for $\theta_0 = 30^\circ$ exhibits 2π periodic behavior due to the reduced symmetry. The most conspicuous feature in Fig. 2(b) is that a clear groove appears in the first branch of the

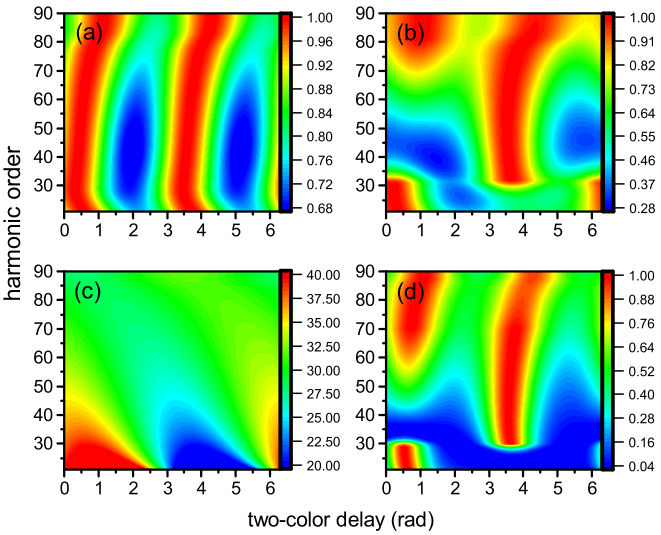

FIG. 2. (a), (b) The normalized HHG intensity distribution from H_2^+ exposed to a two-color laser pulse with $I = 5 \times 10^{14}$ W/cm^2 and $\lambda = 800$ nm at alignment angle (a) $\theta_0 = 0^\circ$ and (b) $\theta_0 = 30^\circ$, respectively. (c) Recollision angles θ (in degrees) obtained by QO theory in the case $\theta_0 = 30^\circ$. Values of angles outside the range of the color scale are shown in the color of the minimum or maximum angle of the scale. (d) The same as (b) but obtained from the tunneling-recombination model.

distribution, which means that the harmonic emission is strongly suppressed in a specific delay and frequency region. The groove is located at higher order compared to the interference minimum in the HHG spectrum generated in the fundamental field only [9]. The reason for this deviation will be clarified below. Our further simulations show that this groove moves to higher harmonic orders as θ_0 is increased. This behavior is in good agreement with that of the minimum caused by the two-center interference. In contrast, the groove in the right side does not correspond to the position of a spectral minimum; it appears mainly because of the normalization procedure and because the intensity in the left branch is much stronger.

To interpret this phenomenon, we model HHG from two-color irradiation by considering the ionization and recombination processes separately. This model is based on the QO model for monochromatic fields. Since the weak second-harmonic field can be taken as a perturbation, the ionization and return times are determined by the fundamental field $E_x(t)$. Neglecting the second-harmonic field in QO model, the ionization time t_1 and return time t_2 of the electron satisfy the saddle-point equations

$$[p_x(t_1, t_2) + A_x(t_1)]^2/2 = I_p, \tag{4a}$$

$$[p_x(t_1, t_2) + A_x(t_2)]^2/2 = \Omega - I_p. \tag{4b}$$

Here $p_x(t_1, t_2) = \frac{-1}{(t_2 - t_1)} \int_{t_1}^{t_2} A_x(t')\, dt'$ is the saddle-point momentum, where $A_x(t) = -\int_0^t E_x(t')\, dt'$. The times t_1 and t_2 are complex valued, and the real part of t_1 is regarded as physical ionization time t_{1i}. Although the times are determined by the fundamental field, the perturbative second-harmonic field modifies the electron trajectory in the y direction. Due to the perturbation, the transverse return velocity is $\upsilon_{y,r} = p_y(t_1, t_2) + A_y(t_2)$, where $p_y(t_1, t_2) = \frac{-1}{(t_2 - t_1)} \int_{t_1}^{t_2} A_y(t')\, dt'$ and $A_y(t)$ is the y component of the vector potential. Similarly, the return velocity along the x direction is $\upsilon_{x,r} = p_x(t_1, t_2) + A_x(t_2)$. Therefore, the electron returns at an angle θ_1 given by $\theta_1 = \arctan(\mathrm{Re}[\upsilon_{y,r}]/\mathrm{Re}[\upsilon_{x,r}])$. Here the real parts of the velocity components are used for the following reason. The complex velocities $\boldsymbol{\upsilon}$ in the QO model are to be understood as those appearing in plane waves of the form $\exp(i\boldsymbol{\upsilon} \cdot \mathbf{r})$. An imaginary part of the complex velocity implies a real term in the exponent and thus modifies the position-dependent amplitude of the wave, not the direction of the wave.

On the other hand, for the electron to recombine to the core at time t_2 it must return to the position it was released at time t_1, i.e., $y(t_2) - y(t_1) = 0$. Hence the transverse initial velocity is

$$\upsilon_{y,i} = \frac{\varepsilon E_0}{2\omega}\left[\cos\varphi_1 + \frac{\sin\varphi_1 - \sin\varphi_2}{2\omega(t_2 - t_1)}\right], \tag{5}$$

where $\varphi_1 = 2\omega t_1 + \phi$ and $\varphi_2 = 2\omega t_2 + \phi$. Inserting t_1 and t_2 from the QO model into Eq. (5), we obtain the initial kinetic energy of the electron as $E_{p,i} = (\mathrm{Re}[\upsilon_{y,i}])^2/2$, which is delay dependent. Then the tunneling rate can be written as

$$\Gamma \propto \exp\left(\frac{-2\{2I_p + (\mathrm{Re}[\upsilon_{y,i}])^2\}^{3/2}}{3|E_x(t_{1i})|}\right), \tag{6}$$

which implies that ionization is strongest for the lowest transverse initial velocity. Here t_{1i} is the real exit time from the QO model. Our extended simulations show that the two-color scan of the HHG intensity from atoms or H_2^+ with $\theta_0 = 0^\circ$ is well reproduced by this tunneling rate model. This suggests that the physical mechanism leading to the groove for $\theta_0 = 30^\circ$ is mainly contained in the recombination process, which is not taken into account in Eqs. (5) and (6).

For H_2^+, the recombination probability is well described by two-center interference following from a plane-wave approximation for the returning electron. Assuming that the active orbital in H_2^+ is a linear combination of atomic orbitals [23], the velocity-form recombination matrix element [24] is proportional to $\cos[k(R/2)\cos\theta]$, and the recombination probability is $R_{\mathrm{rec}}(R, \theta) \propto |\cos[k(R/2)\cos\theta]|^2$. Here the simple heuristic formula $k = \sqrt{2\Omega}$ is used as effective momentum that considers the Coulomb effect, and θ is the recollision angle relative to the molecular axis. Considering the transverse offset caused by the second-harmonic field, the recollision angle is $\theta = |\theta_1 - \theta_0|$. Figure 2(c) shows the recollision angle θ obtained from the QO model as a function of two-color delay and harmonic order. For our parameters, the angle θ_1 is up to $\pm 25^\circ$ at certain delays for the lowest harmonic order, but it decreases quickly for higher orders. It is shown that, compared with $\theta_0 = 30^\circ$, the recollision angle θ is increased in the first branch but decreased in the second one, especially in the lower orders. Since the interference minimum corresponds to $R_{\mathrm{rec}}(R, \theta) = 0$ i.e., $kR\cos\theta = (2n + 1)\pi$, the minimum moves upwards (downwards) in the first (second) branch, which explains the groove in Fig. 2(b). The recollision angle of electrons is modulated by the second-harmonic field, thus the interference effect is tuned by the

two-color delay. Therefore, the harmonic intensity from H_2^+ can be expressed as a product of the tunneling rate and recombination probability:

$$I_{\rm harm} \propto \exp\left[\frac{-4\sqrt{2}(I_p + E_{p,i})^{3/2}}{3|E_x(t_{1i})|}\right] R_{\rm rec}(R, \theta). \quad (7)$$

This model is named as tunneling-recombination model in the following. The result of Eq. (7) is shown in Fig. 2(d). It is striking that the whole distribution is in good qualitative agreement with the TDSE result. Therefore, the perturbative second-harmonic field plays a significant role in both ionization and recombination. The two-color delay modifies the ionization rate leading to a two-branch structure in the HHG intensity distribution. Simultaneously, this delay tunes the position of the interference minimum. The interplay of these two effects implies that the ionization-time retrieval [6,17] cannot be readily applied when $\theta_0 \neq 0$.

B. Asymmetric molecular ions and Gaussian recollision

In the following, we extend our discussion to asymmetric molecular ions to explore the role of asymmetry in two-color HHG. We start our discussion with a model HeH^{2+} ion with effective charges $Z_{\rm He}/Z_{\rm H} = 2$. All other molecular and field parameters are the same as those used for H_2^+ above. In particular, the charges are chosen to reproduce the same ionization potential $I_p = 1.1$ a.u. as in H_2^+ while keeping the ratio as 2:1. While this is not the true ionization potential of HeH^{2+}, it has the advantage of providing a more direct comparison with the H_2^+ results. First, as illustrated in panel A of Fig. 1(b), the internuclear vector pointing from the heavy nucleus to the light nucleus is oriented at an angle of 30° relative to the x direction (the polarization axis of the fundamental field). In this case, the tunneling occurs on the helium side, and the basic properties of the HHG intensity distribution [see Fig. 3(a)] are similar to that of H_2^+, except that the groove is not as pronounced as for H_2^+. If we assume the groove also to be an interference effect, the result means that the groove becomes shallower because the destructive interference between contributions from the two centers do not completely cancel each other. When the molecular axis is reversed (the orientation angle becomes $\theta_0 = -150°$), the tunneling switches to the hydrogen side. The harmonic emission is strongly suppressed in most harmonic orders in the first branch of the distribution, and the interference groove becomes unobservable. In other words, the HHG intensity shows an obvious orientation asymmetry.

For completeness, we proceed with a similar calculation on the more realistic case of a HeH^+ ion. Since the bound electrons are localized on the helium side, we assume a partial screening of the helium atom. The soft-core potential is written then as

$$V(\mathbf{r}) = -\frac{Z_{\rm H}}{\sqrt{r_{\rm H}^2 + \xi}} - \frac{\left(Z_{\rm He}^{\rm in} - Z_{\rm He}^{\rm out}\right)\exp\left(-r_{\rm He}^2/\rho\right) + Z_{\rm He}^{\rm out}}{\sqrt{r_{\rm He}^2 + \xi}}. \quad (8)$$

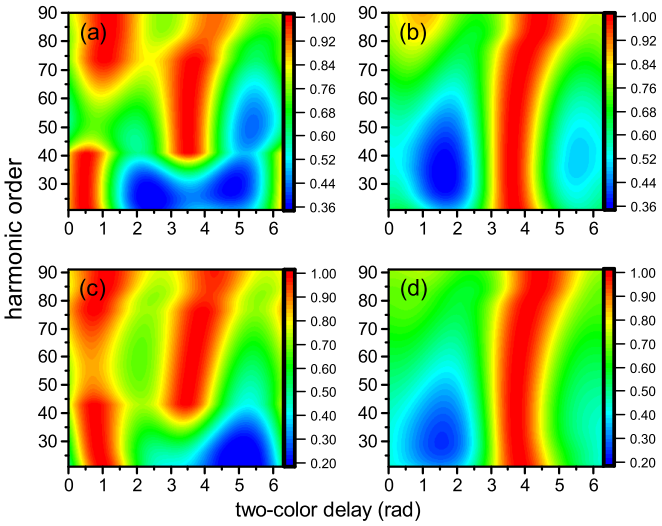

FIG. 3. In panels (a) and (b), we show the two-color delay scan of the HHG intensity for model HeH^{2+} at orientation angle $\theta_0 = 30°$ and $\theta_0 = -150°$, respectively. The laser parameters are the same as those used in Fig. 2. In panels (c) and (d) we show the harmonic intensity distributions for HeH^+ at $\theta_0 = 30°$ and $\theta_0 = -150°$, when the intensity and wavelength of the fundamental field are chosen as $I = 1.2 \times 10^{15}$ W/cm^2 and $\lambda = 600$ nm.

Here $Z_{\rm H} = 1$ is the nuclear charge of hydrogen, and $Z_{\rm He}^{\rm in} = 2$ and $Z_{\rm He}^{\rm out} = 1$ denote the inner and outer limit of the effective charge for helium. The internuclear distance is set to be $R = 1.8$ a.u., a little larger than the equilibrium distance $R = 1.4$ a.u. This serves for better comparability with the other systems studied above. The screening parameter ρ is adjusted such that the ionization potential is $I_p = 1.5055$ a.u. Due to the large value of the ionization potential, a higher intensity is used to obtain significant ionization. At the same time, a higher frequency is used to avoid an increase of the harmonic cutoff energy. The field strength and the frequency are chosen to be $E_0 = 0.174$ a.u. and $\omega = 0.07593$ a.u. corresponding to an intensity of $I = 1.2 \times 10^{15}$W/cm^2 and a wavelength $\lambda = 600$ nm, respectively. The two-color delay scans for HeH^+ in Figs. 3(c) and 3(d) exhibit similar phenomena as for HeH^{2+}. However, the groove becomes even shallower for the helium-side tunneling case, and the suppression of harmonic emission seems even stronger in the first branch for the hydrogen-side case.

To explain the orientation asymmetry, field-free collisions of Gaussian wave packets are implemented to simulate the recombination step in harmonic generation [9,18]. The initial wave packet $\Psi(\mathbf{r})$ is given by a superposition of the ground state $\Psi_0(\mathbf{r})$ and a Gaussian wave packet $\Psi_G(\mathbf{r})$: $\Psi(\mathbf{r}) = [\Psi_0(\mathbf{r}) + \Psi_G(\mathbf{r})]/\sqrt{2}$. In order to simulate the two-color delay scan scheme, the Gaussian wave packet mimics the returning electron. For each delay, the wave packet is set to move toward the molecule (also the grid center) from the direction $\theta = |\theta_1 - \theta_0|$ relative to the molecular axis. The recollision angle θ is exactly the same as we used in the tunneling-recombination model. The spatial grid size is $L_x \times L_y = 400 \times 400$ a.u. with 1024×1024 grid points. The propagation time is one optical period T with 2048 time steps. When the center momentum is chosen to be $k_0 = \sqrt{2(\Omega - I_p)}$ the initial center position of the

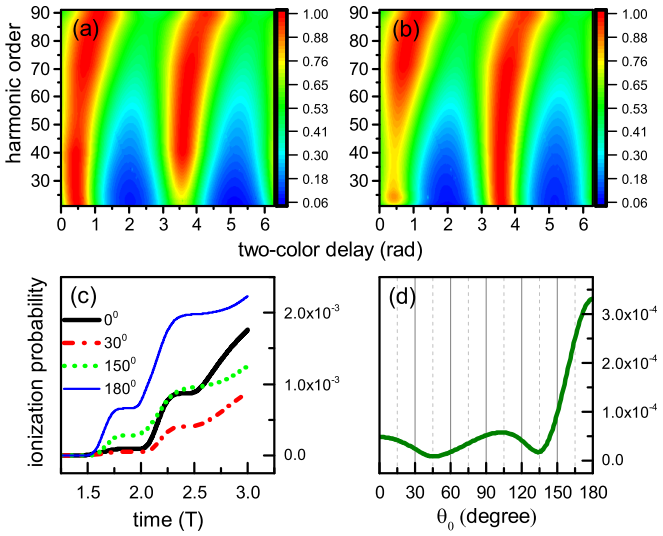

FIG. 4. (a), (b) The Gaussian collision results for HeH^+ obtained using Eq. (9) corresponding to Figs. 3(c) and 3(d). (c) Ionization probabilities as a function of time at different orientation angles. (d) Orientation dependence of the ionization yield in the time interval $[1.40T, 1.65T]$.

Gaussian wave packet is set to $r_0 = Tk_0/2$ from the grid center. Once the dipole acceleration has been obtained, Fourier transforms are performed to calculate spectra $S_{\text{Gauss}}(\Omega, \phi)$. Combining these spectra with the tunneling rate Γ, we model the harmonic intensity as

$$I_{\text{harm}} \propto \exp\left[\frac{-4\sqrt{2}(I_p + E_{p,i})^{3/2}}{3|E_x(t_{1i})|}\right] S_{\text{Gauss}}(\Omega, \phi). \quad (9)$$

Figures 4(a) and 4(b) give examples of the Gaussian collision results of HeH^+ corresponding to the TDSE results in Figs. 3(c) and 3(d). The basic features of orientation asymmetry such as the groove and the suppression visible in the TDSE results are not well reproduced, suggesting that the recombination process plays only a partial role in the orientation asymmetry. This situation motivates our consideration of the orientation dependence in the ionization process, which has been discussed previously as a permanent dipole effect [25,26].

For investigation of the ionization process, we turn off the second-harmonic field, so that the HeH^+ molecule is exposed to a linearly polarized field only. Numerically, the ionization probability $P(t)$ is evaluated as the decay of the norm of the wave function at time t due to the removal of the continuum electron at the grid boundary, $P(t) = 1 - \langle\Psi(t)|\Psi(t)\rangle$. In Fig. 4(c) ionization probabilities at a few orientation angles are plotted, showing an obvious orientation dependence. As one may expect, the ionization is strongest when the field is antiparallel to the internuclear vector ($\theta_0 = 180°$) such that tunneling via hydrogen takes place, which is much stronger than ionization in the parallel case when tunneling from helium takes place ($\theta_0 = 0°$). It is worth noticing that this probability is counted at the time t when the tunneled electrons reach the grid boundary ($x, y = \pm L_{x,y}/2$), while the exit time t_{1i} discussed above is defined as the time when the electron exits the tunneling barrier. The time delay $\Delta t = t - t_{1i}$ between time t and the exit time t_{1i} can be estimated from TDSE calculations. For HeH^+ at our laser parameters, we find a time delay about $\Delta t = 0.15T$. Since the exit time corresponding to the Gabor analysis region is in an interval $[1.25T, 1.50T]$, the electrons reach the boundary in a time region $[1.40T, 1.65T]$. Thus we evaluate the ionization yield as $P_{\text{ion}} = P(1.65T) - P(1.40T)$ and plot P_{ion} as a function of orientation angle in Fig. 4(d). This shows that the ionization yield varies considerably when the orientation angle is varied around $\theta_0 = 30°$ (tunneling on the helium side) or around $\theta_0 = 150°$ (tunneling on the hydrogen side). This could give an explanation of the orientation asymmetry in the TDSE results. Due to the perturbation by the second-harmonic field, the direction of the ionizing field is slightly modified. When the orientation is $\theta_0 = -150°$, as in Figs. 3(b) and 3(d), the angle of the ionizing field becomes less than 150° in the first branch and the ionization yield decreases rapidly, so that the harmonic emission is suppressed, especially at low orders. For $\theta_0 = 30°$ [Figs. 3(a) and 3(c)], the harmonic intensity is affected less, due to the weaker orientation dependence of ionization. Thus an interference groove can be observed in the two-color delay scan, which is similar to the case of symmetric molecules. We conclude that the orientation dependence of HHG from asymmetric molecules in a two-color field is strongly influenced by the orientation dependence of ionization. We believe that additional effects such as orientation-dependent return probabilities [27] may play a role, which are outside the scope of the present model.

IV. CONCLUSION

In summary, we have investigated HHG from models of diatomic molecules including the symmetric molecular ion H_2^+ and asymmetric molecular ions HeH^{2+} and HeH^+ in orthogonally polarized two-color fields by solving the time-dependent Schrödinger equation. Our simulations show that two-center interference effects can be observed both for H_2^+ and for the asymmetric systems if tunneling takes place on the helium side. A groove appears in the HHG intensity as a function of delay and harmonic order. Considering the effect of the two-color delay both in ionization and recombination processes, we explain the HHG intensity from H_2^+ with the help of the QO model, which can well reproduce the TDSE results. To interpret the orientation asymmetry in HHG from the asymmetric molecules, the field-free collision of Gaussian wave packets is implemented as a way to include the orientation dependence of recombination. The orientation dependence of ionization is also discussed. We mention that all the above analysis is restricted to HHG coming from short trajectories that are born in one half laser cycle. To observe these findings, one would need an ultrashort few-cycle pulse so that only one branch of short trajectories contributes to the measured HHG signal.

Before concluding, we mention that the orientation dependence of HHG from asymmetric molecules can be observed already in harmonic spectra generated by the fundamental field only. In the time-frequency distribution, the groove related to the two-center interference can be observed only when the tunneling occurs on the helium side, where the harmonic

emission is weaker than the hydrogen side case [28]. By introducing the second-harmonic field and tuning the two-color delay, not only is the position of interference groove modified, but also the appearance of the groove can be controlled in asymmetric molecules. Our work thus sheds light on the roles of the ionization and recollision processes in HHG from diatomic molecules.

ACKNOWLEDGMENTS

This work was supported by the National Natural Science Foundation of China (Grant No. 11504069) and grant provided by the China Scholarship Council (CSC). We thank the Deutsche Forschungsgemeinschaft for support within the Priority Programme "Quantum Dynamics in Tailored Intense Fields" (QUTIF).

[1] P. B. Corkum and F. Krausz, Attosecond science, Nat. Phys. **3**, 381 (2007).

[2] P. B. Corkum, Plasma Perspective on Strong-Field Mutiphoton Ionization, Phys. Rev. Lett. **71**, 1994 (1993).

[3] M. Lewenstein, P. Balcou, M. Yu. Ivanov, A. L'Huillier, and P. B. Corkum, Theory of high-harmonic generation by low-frequency laser fields, Phys. Rev. A **49**, 2117 (1994).

[4] P. Salieres, B. Carre, L. Le Deroff, F. Grasbon, G. G. Paulus, H. Walther, R. Kopold, W. Becker, D. B. Milosevic, A. Sanpera, and M. Lewenstein, Feynman's path-integral approach for intense-laser-atom interactions, Science **292**, 902 (2001).

[5] Y. Mairesse, A. de Bohan, L. J. Frasinski, H. Merdji, L. C. Dinu, P. Monchicourt, P. Breger, M. Kovačev, R. Taïeb, B. Carré, H. G. Muller, P. Agostini, and P. Salières, Attosecond synchronization of high-harmonic soft x-rays, Science **302**, 1540 (2003).

[6] J. Zhao and M. Lein, Determination of Ionization and Tunneling Times in High-Order Harmonic Generation, Phys. Rev. Lett. **111**, 043901 (2013).

[7] J. Itatani, J. Levesque, D. Zeidler, H. Niikura, H. Pepin, J. C. Kieffer, P. B. Corkum, and D. M. Villeneuve, Tomographic imaging of molecular orbitals, Nature (London) **432**, 867 (2004).

[8] S. Haessler, J. Caillat, W. Boutu, C. Giovanetti-Teixeira, T. Ruchon, T. Auguste, Z. Diveki, P. Breger, A. Maquet, B. Carré, R. Taeb, and P. Salières, Attosecond imaging of molecular electronic wavepackets, Nat. Phys. **6**, 200 (2010).

[9] M. Lein, N. Hay, R. Velotta, J. P. Marangos, and P. L. Knight, Role of the Intramolecular Phase in High-Harmonic Generation, Phys. Rev. Lett. **88**, 183903 (2002).

[10] W. Boutu, S. Haessler, H. Merdji, P. Breger, G. Waters, M. Stankiewicz, L. J. Frasinski, R. Taieb, J. Caillat, A. Maquet, P. Monchicourt, B. Carre, and P. Salieres, Coherent control of attosecond emission from aligned molecules, Nat. Phys. **4**, 545 (2008).

[11] C. Vozzi, F. Calegari, E. Benedetti, J. P. Caumes, G. Sansone, S. Stagira, M. Nisoli, R. Torres, E. Heesel, N. Kajumba, J. P. Marangos, C. Altucci, and R. Velotta, Controlling Two-Center Interference in Molecular High Harmonic Generation, Phys. Rev. Lett. **95**, 153902 (2005).

[12] R. Velotta, N. Hay, M. B. Mason, M. Castillejo, and J. P. Marangos, High-Order Harmonic Generation in Aligned Molecules, Phys. Rev. Lett. **87**, 183901 (2001).

[13] M. Lein, Molecular imaging using recolliding electrons, J. Phys. B **40**, R135 (2007).

[14] M. Kitzler and M. Lezius, Spatial Control of Recollision Wave Packets with Attosecond Precision, Phys. Rev. Lett. **95**, 253001 (2005).

[15] M. Kitzler, X. Xie, A. Scrinzi, and A. Baltuska, Optical attosecond mapping by polarization selective detection, Phys. Rev. A **76**, 011801(R) (2007).

[16] M. Murakami, O. Korobkin, and M. Horbatsch, High-harmonic generation from hydrogen atoms driven by two-color mutually orthogonal laser fields, Phys. Rev. A **88**, 063419 (2013).

[17] D. Shafir, H. Soifer, B. D. Bruner, M. Dagan, Y. Mairesse, S. Patchkovskii, M. Y. Ivanov, O. Smirnova, and N. Dudovich, Resolving the time when an electron exits a tunneling barrier, Nature (London) **485**, 343 (2012).

[18] E. V. van der Zwan and M. Lein, Two-center interference and ellipticity in high-order harmonic generation from H_2^+, Phys. Rev. A **82**, 033405 (2010).

[19] M. D. Feit, J. A. Fleck, Jr., and A. Steiger, Solution of the Schrödinger equation by a spectral method, J. Comput. Phys. **47**, 412 (1982).

[20] V. V. Strelkov, M. A. Khokhlova, A. A. Gonoskov, I. A. Gonoskov, and M. Yu. Ryabikin, High-order harmonic generation by atoms in an elliptically polarized laser field: Harmonic polarization properties and laser threshold ellipticity, Phys. Rev. A **86**, 013404 (2012).

[21] J. J. Carrera, X. M. Tong, and S.-I. Chu, Creation and control of a single coherent attosecond xuv pulse by few-cycle intense laser pulses, Phys. Rev. A **74**, 023404 (2006).

[22] C. C. Chirilă, I. Dreissigacker, E. V. van der Zwan, and M. Lein, Emission times in high-order harmonic generation, Phys. Rev. A **81**, 033412 (2010).

[23] I. N. Levine, *Quantum Chemistry*, 7th ed. (Pearson, New York, 2014).

[24] C. C. Chirilă and M. Lein, Assessing different forms of the strong-field approximation for harmonic generation in molecules, J. Mod. Opt. **54**, 1039 (2007).

[25] G. Lagmago Kamta and A. D. Bandrauk, Phase Dependence of Enhanced Ionization in Asymmetric Molecules, Phys. Rev. Lett. **94**, 203003 (2005).

[26] E. Dehghanian, A. D. Bandrauk, and G. Lagmago Kamta, Enhanced ionization of the non-symmetric HeH^+ molecule driven by intense ultrashort laser pulses, J. Chem. Phys. **139**, 084315 (2013)

[27] F. Schell, T. Bredtmann, C. P. Schulz, S. Patchkovskii, M. J. J. Vrakking, and J. Mikosch, Molecular orbital imprint in laser-driven electron recollision, Sci. Adv. **4**, eaap8148 (2018).

[28] B. Zhang, S. Yu, Y. Chen, X. Jiang, and X. Sun, Time-resolved dynamics of odd and even harmonic emission from oriented asymmetric molecules, Phys. Rev. A **92**, 053833 (2015).